

## 1 Highlights

### 2 **Spatial Disaggregation of Particulate Matter Emission Inventory in the Metropolitan Area** 3 **of Aburrá Valley for Air Quality Modelling**

4 Santiago Lopez-Restrepo, Andres Yarce, Nicolás Pinel, O. L. Quintero, Arjo Segers, A. W. Heemink

- 5 • A new emission inventory, the main uncertainty source in air quality studies, has been estimated using a top-  
6 down spatial disaggregation methodology.
- 7 • Using this local emission inventory, model simulations of particulate matter improve.
- 8 • Application of an air quality simulation over Colombia.
- 9 • High-Resolution Chemical Transport Model LOTOS-EUROS has been configured for the Aburrá Valley.

# Spatial Disaggregation of Particulate Matter Emission Inventory in the Metropolitan Area of Aburrá Valley for Air Quality Modelling

Santiago Lopez-Restrepo<sup>a,d,\*</sup>, Andres Yarce<sup>a,c,d</sup>, Nicolás Pinel<sup>b,c</sup>, O. L. Quintero<sup>a</sup>, Arjo Segers<sup>e</sup> and A. W. Heemink<sup>d</sup>

<sup>a</sup>Mathematical Modelling Research Group, Universidad EAFIT, Medellín, Colombia

<sup>b</sup>Department of Biological Sciences, Universidad EAFIT, Medellín, Colombia

<sup>c</sup>Biodiversity, Evolution and Conservation Research Group, Universidad EAFIT, Medellín, Colombia

<sup>d</sup>Department of Applied Mathematics, TU Delft, Delft, The Netherlands

<sup>e</sup>Department of Climate, Air and Sustainability, TNO, Utrecht, The Netherlands

## ARTICLE INFO

### Keywords:

Air quality modelling  
Top-down emission inventory  
Chemical transport model  
Particulate Matter  
Local emissions inventory  
LOTOS-EUROS

## ABSTRACT

In this paper a local emission inventory for PM<sub>10</sub> and PM<sub>2.5</sub> is presented that has been developed using a top-down spatial disaggregation of the official emission inventory for the Metropolitan Area of the Aburrá Valley in Colombia. The local emission inventory was evaluated using the LOTOS-EUROS Chemical Transport Model in a high-resolution simulation, and compared with the global emission inventory EDGAR. A detailed analysis of the model using the local emission inventory was performed. The results showed a considerable improvement in model performance when the local emission inventory was used in comparison to the global emission inventory.


## 1. Introduction

Air pollution has become one of the most important concerns of local authorities of growing cities in Latin American (Kumar, Jiménez, Belalcázar and Rojas, 2016). Emissions from urban agglomerations are major sources of regional and global atmospheric pollution (Green and Sánchez, 2012). An example of this is the Aburrá Valley that constitutes the second most populous metropolitan area in Colombia. It is composed of the city of Medellín and its neighboring municipalities. Within the Aburrá Valley, air quality conditions deteriorate with the overpass of the 1 Intertropical Convergence Zone (March-April, and with lower intensity in October-November). During the overpass, the atmospheric boundary layer stays often below the rim of the canyon, trapping the pollutants within the valley (Jiménez, 2016).

Due to the large stress on human health induced by this air pollution, efforts have been made to monitor, reduce, and prevent episodes in which concentrations of pollutants reach hazard levels. Before measures for reducing air pollution can be implemented it is important to know the actual concentration levels and how these evolve in time over the area of interest. This could be done using a Chemical Transport Model (CTM) to simulate concentrations of trace gasses and particulate matter (Thunis, Miranda, Baldasano, Blond, Douros, Graff, Janssen, Juda-Rezler, Karvosenoja, Maffei, Martilli, Rasoloharimahefa, Real, Viaene, Volta and White, 2016; Lateb, Meroney, Yataghene, Fellouah, Saleh and Boufadel, 2016).

An early study on atmospheric pollution in Colombia used the WRF-CHEM model (Weather Research and Forecasting with Chemistry) to simulate the concentrations of PM<sub>10</sub> over the Bogotá metropolitan area (Kumar et al., 2016). The EDGAR (Emissions Database for Global Atmospheric Research) global emission inventory was used as input. The simulations underestimated the PM<sub>10</sub> concentrations by an order of magnitude compared to observations. The WRF-CHEM model has also been applied to study the behavior of O<sub>3</sub> over the medium-size, mountainous city of Manizales (González, Ynoue, Vara-Vela, Rojas and Aristizábal, 2018). By using high-resolution simulations (1x1 km), the study compared the performance of the model when using either the EDGAR emission inventory or a high-resolution emission inventory previously developed (Gonzalez, Gomez, Rojas, Acevedo and Aristizabal, 2017). This study showed a significant improvement of the model performance when using the high-resolution emission inventory.

\*Corresponding author

 slopezr2@eafit.edu.co, s.lopezrestrepo@tudelft.nl (S. Lopez-Restrepo)

ORCID(s): 0000-0002-7637-1575 (S. Lopez-Restrepo); 0000-0003-1441-2367 (A. Yarce); 0000-0003-1304-3096 (N. Pinel); 0000-0002-8697-4361 (O.L. Quintero); 0000-0002-1319-0195 (A. Segers); 0000-0001-8559-9566 (A.W. Heemink)

For the city of Medellín, a similar under estimation of  $PM_{2.5}$  and  $PM_{10}$  concentrations has been observed for simulations with the LOTOS-EUROS CTM (Lopez-Restrepo, Yarce, Pinel, Quintero, Segers and Heemink, 2020), which also used the global EDGAR inventory as input. Data assimilation was used to adjust the emissions, and due to the persistent low bias the best performance was obtained by strongly increasing the emissions over the entire domain. Despite repeated studies showing that the EDGAR inventory has its limitations for application over Colombian (Gonzalez et al., 2017; Pachón, Galvis, Lombana, Carmona, Fajardo, Rincón, Meneses, Chaparro, Nedbor-Gross and Henderson, 2018; Nedbor-Gross, Henderson, Pérez-Peña and Pachón, 2018), this database is still the only one available that includes all species necessary for air quality simulations over a large region of the northeast Andes domain.

In this paper, a disaggregation methodology is proposed to create a local map of particulate matter (PM) emissions that is suitable for modelling purposes. The emissions are based on the current official emission inventory for the Metropolitan Area of the Aburrá Valley. The new emission inventory is compared with the global emission inventory EDGAR v4.3 (Crippa, Guizzardi, Muntean, Schaaf, Dentener, van Aardenne, Monni, Doering, Olivier, Pagliari and Janssens-Maenhout, 2018), and used in simulations with the LOTOS-EUROS model. The simulated particulate matter concentrations are compared with observations from surface stations from a local air quality network.

The paper is organized as follows. Section 2 presents the relevant information regarding the emission data and how the new emission inventory was built. The simulation model, observations and methodology used to validate the simulations are also presented. Section 3 shows the local emission inventory and a comparison with the EDGAR v4.3 emissions. In this section the simulated PM concentrations are evaluated for two different periods using both the new local inventory as well as the original global inventory. Section 4 summarizes the main conclusions and provides an outlook for future research.

## 2. Materials and methods

### 2.1. Local emission inventories

The base of the new emission map is formed by an on-road vehicular and industrial point-source inventory developed by the Área Metropolitana del Vallé de Aburrá (AMVA) in cooperation with the Universidad Pontificia Bolivariana located in Medellín, Colombia (UPB and AMVA, 2017)<sup>1</sup>. The inventory was initially created for 2015 and updated in 2016. The database covers the 10 municipalities that together constitute the Metropolitan Area of the Aburrá Valley shown in Figure 5. The AMVA emission inventory provides a complete set of emitted trace gases such as carbon monoxide (CO), nitrogen oxides ( $NO_x$ ), sulphuric oxides ( $SO_x$ ), and volatile organic compounds (VOC's), as well as particulate matter with diameters less than  $2.5 \mu m$  ( $PM_{2.5}$ ) or less than  $10 \mu m$  ( $PM_{10}$ ). The particulate matter emissions form the largest contribution to the air quality deterioration in the Valley (Hoyos, Herrera-Mejía, Roldán-Henao and Isaza, 2019), and these are therefore the focus of this study. The AMVA inventory followed a bottom-up methodology, combining activity data (traffic intensities, industrial production) with emission factors. Only traffic and industrial point sources are considered, neither household or commercial sources are taken into account.

#### 2.1.1. Traffic emissions

The data for the traffic emissions in the AMVA inventory originates from the mobility offices at all ten municipalities of the Valley. Five vehicle categories are distinguished: passenger cars, taxis, buses, trucks (including tractor and tipper trucks), and motorcycles (subdivided in two groups with different engine capacity and type of motor, namely 2-stroke motors  $< 100$  cc; and 4-stroke motors ( $cc < 100, 100 < cc < 300, 300 < cc$ )). The total number of registered vehicles in the metropolitan area for 2016 was 1.3 million. Figure 1 shows the total number of vehicles by category, and the corresponding type of fuel used. Despite motorcycles being the dominant category, their overall contribution to emissions is lower than diesel-fueled trucks.

The total emissions for  $PM_{10}$  and  $PM_{2.5}$  by vehicle category for the year 2016 are shown in Figure 2 (a). The total yearly contribution of  $PM_{2.5}$  is higher than that of  $PM_{10}$ . While trucks dominate in the emissions of  $PM_{2.5}$ , passenger cars are the main source of vehicular  $PM_{10}$ .

#### 2.1.2. Point source emissions

Data for industrial point-source emissions had been collected from large and medium-size industrial facilities within the Aburrá Valley. Information for 12 different industrial activities was gathered from the official reporting to the environmental agency. Of these, eight economic activities that represent more than 98% of the total emissions are taken into

<sup>1</sup>available from <https://www.metropol.gov.co/ambiental/calidad-del-aire/Documents/Inventario-de-emisiones>

### Spatial Disaggregation of Particulate Matter Emissions

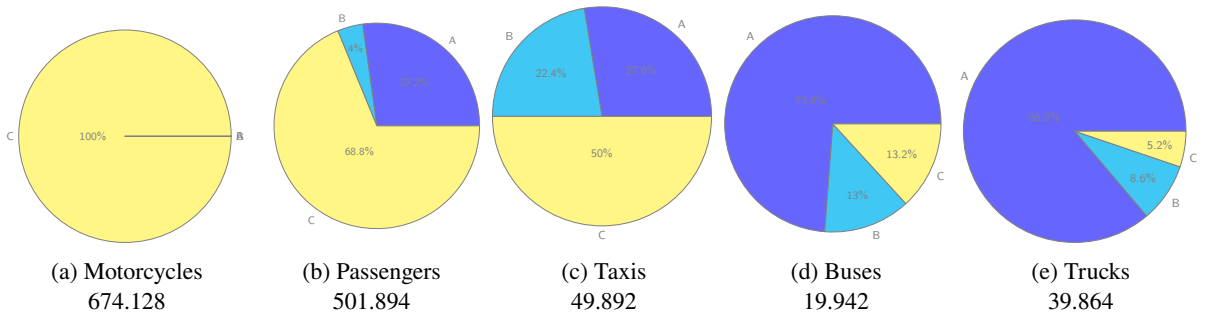


**Figure 1:** Total number of mobile sources per category, and subdivision of mobile sources in terms of type of fuel: A - Diesel, B-Natural Gas, and C-Gasoline.

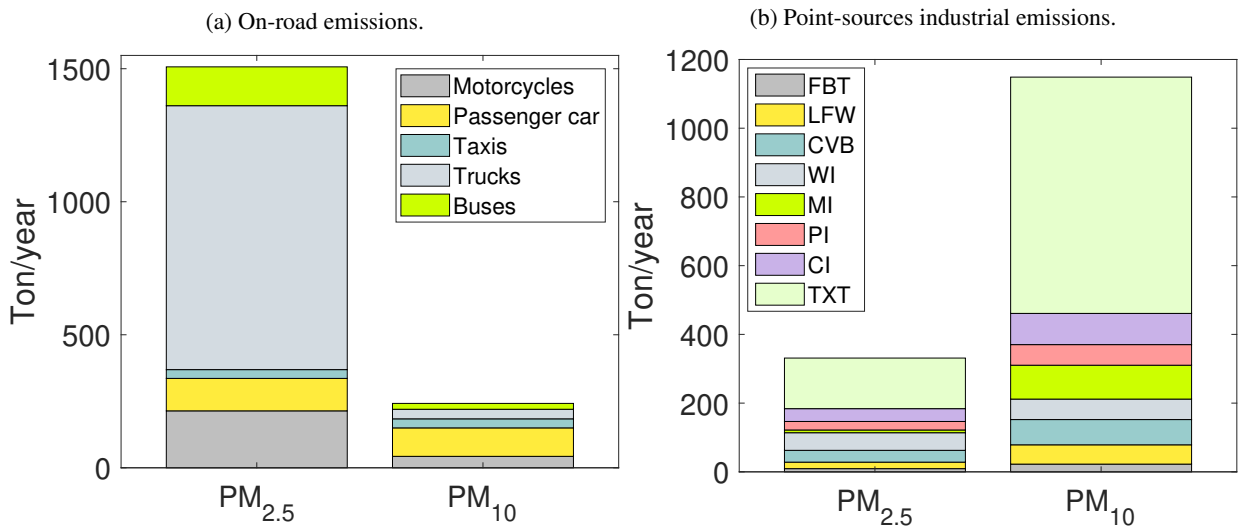


**Figure 2:** Total PM<sub>10</sub> and PM<sub>2.5</sub> emissions in the AMVA inventory for the five vehicle categories (a), and the particulate matter emissions from industrial point sources (b).

104 account in this study: 1) Food, Beverage and Tobacco (FBT); 2) Leather and Footwear (LFW); 3) Ceramic, Vitreous,  
 105 Brick Makers, Potters, Tiles and Ceramic industries (CVB); 4) Wood industry (WdI); 5) Metallurgical industry (MI);  
 106 6) Paper Industry (PI); 7) Chemical industry (CI); and 8) Textiles (TXT). Emission factors that define the emission  
 107 strength given unit of production were taken from the EPA AP-42 report (US EPA (United State Environmental Pro-  
 108 tection Agency), 1995) and applied for each industrial facility based on the reported type of fuel, type of combustion  
 109 equipment, and firing configuration. The information included in the AMVA inventory covered 432 industrial facili-  
 110 ties and 1448 emission point sources. The annual emission total for PM<sub>10</sub> and PM<sub>2.5</sub> by economic activity is shown  
 111 in Figure 2(b), which was calculated from the activity level of the industry, the emission factor, but was partly also  
 112 based on direct sampling campaigns. The TXT, MI, FBT and CI sectors are responsible for the majority of industrial  
 113 emissions, with TXT contributing the largest amount. The Wood Industry is the second largest producer of PM<sub>2.5</sub>  
 114 pollution, despite that the sector occupies just 2 percent of the point sources and 3 percent of all the industrial sites in  
 115 the inventory.

## 2.2. Temporal disaggregation

116 To be able to use the AMVA emission information in a simulation model, it is necessary to expand it with a temporal  
 117 profile. The temporal profile distributes a yearly total emission over seasons (months), days (work days or weekends),  
 118 and hours of the day. For road-traffic emissions, a daily profile following the traffic density for a working day in  
 119 the metropolitan area was taken from (UPB and AMVA, 2017). This profile has an hourly resolution, as shown in  
 120 Figure 4. Industrial emissions can have a strong variability within a day, but since no detailed information is available,  
 121

### Spatial Disaggregation of Particulate Matter Emissions

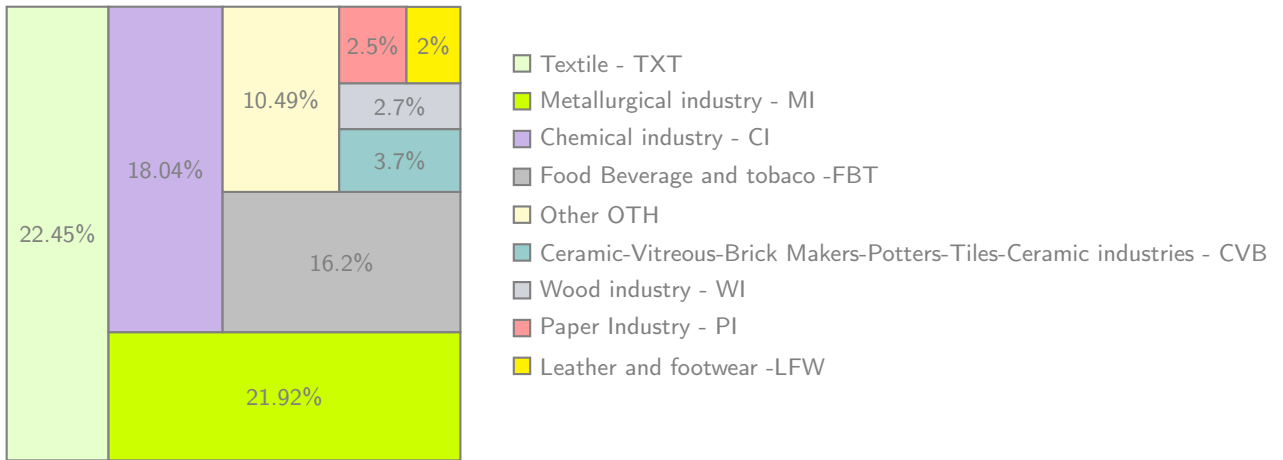


Figure 3: Percentage of industrial facilities per economy activities.

122 their temporal profile is kept constant in this study.

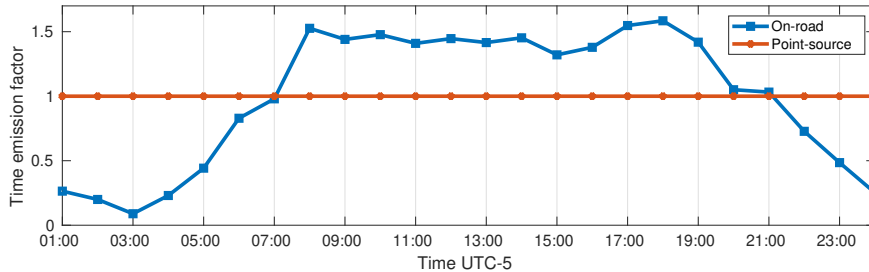


Figure 4: Temporal emission profiles used for traffic and industrial point source emissions.

### 123 2.3. Spatial disaggregation

124 Apart from a temporal profile, a simulation model also requires a spatial disaggregation. The result is a map of  
 125 emission intensities that shows spatial differences in emission strengths; the total sum should equal the inventory data.

126 The AMVA inventory was disaggregated over the Metropolitan Area of the Aburrá Valley ( 76°W-75°W and 5.7°N-  
 127 6.8°N ) at a resolution of 0.01°×0.01°(approximately 1 km × 1 km). Disaggregation methods use variables such as land  
 128 use and population density maps, traffic counts, and simplified and complete road networks to assign emissions to grid  
 129 cells (Saide, Zah, Osses and Ossés de Eicker, 2009). A Disaggregation Factor (DF) can be derived from normalized  
 130 weights for each cell in the domain based on specific information such as traffic intensity or road density (Saide et al.,  
 131 2009; Shu and Lam Nina, 2011).

132 In this study, a method based on road density was implemented following (Ossés de Eicker, Zah, Triviño and  
 133 Hurni, 2008). The road network map was obtained from the OpenStreetMap database (Haklay and Weber, 2008), and  
 134 simplified by removing the segments classified as residential, as recommended in (Tuia, Ossés de Eicker, Zah, Osses,  
 135 Zarate and Clappier, 2007; Gómez, González, Osses and Aristizábal, 2018). The simplification of the road network  
 136 can reduce errors in the spatial disaggregation since normally residential roads correspond to a high portion of the road  
 137 network length but carry a low percentage of vehicular traffic (Gonzalez et al., 2017). Although this method is one of  
 138 the simplest disaggregation methods, it has been shown as a valuable method for high-density cities (as is the case of  
 139 the Metropolitan Area of the Aburrá Valley), and in applications where detailed information about traffic intensity is  
 140 not available (Tuia et al., 2007).

For each grid cell  $j$ , the corresponding  $DF$  was calculated with (Ossés de Eicker et al., 2008):

$$DF_j = \frac{\sum_{i=0}^I S_{i,j}}{\sum_{j=0}^J \sum_{i=0}^I S_{i,j}} \quad (1)$$

141 where  $S_{i,j}$  is the road segment  $i$  in the grid cell  $j$ ,  $I$  is the total length of road segments in each grid cell, and  $J$  is  
 142 the total number of grid cells. Figure 5 shows the simplified road network map used for the on-road spatial disaggregation.

143 The point-source emissions were distributed on the grid using their known location, obtained from the official  
 144 emissions inventory (UPB and AMVA, 2017).

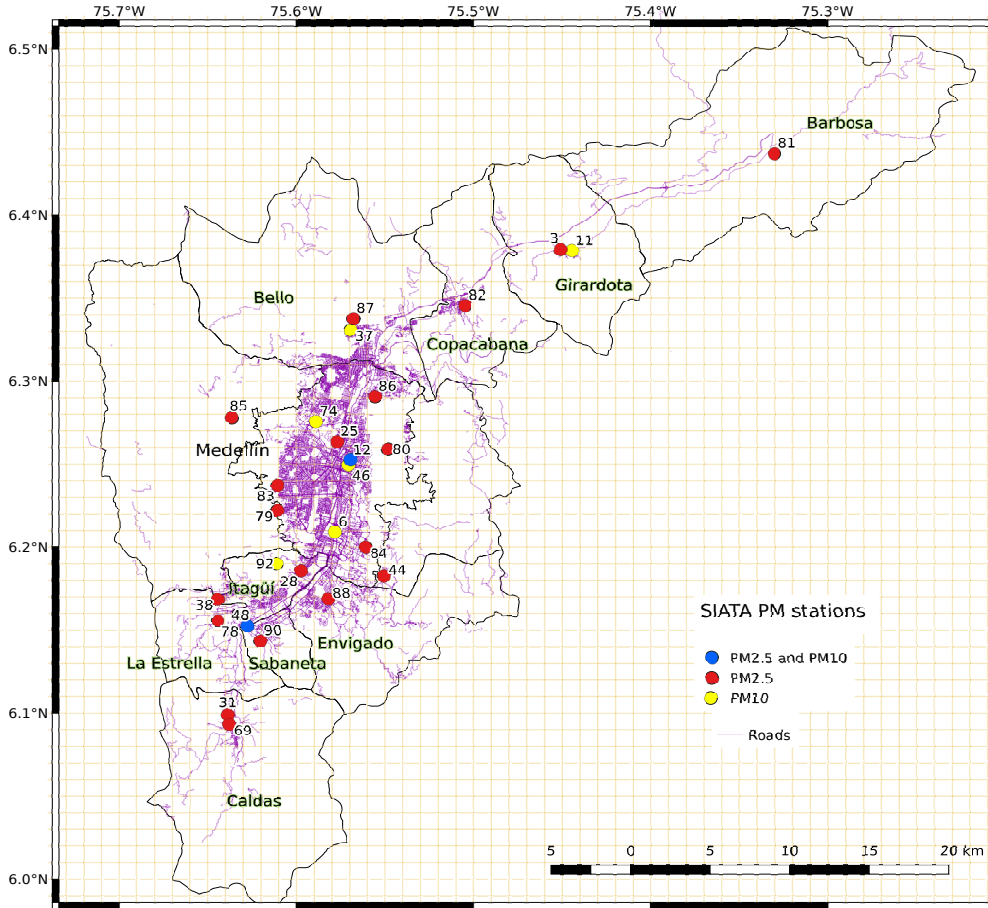


Figure 5: Simplified road network of the Metropolitan Area of the Aburrá Valley and SIATA particulate matter station distribution. The raster corresponds to the chosen emission grid.

145 **2.4. LOTOS-EUROS model**

146 The LOTOS-EUROS (LONg Term Ozone Simulation - EUROpean Operational Smog) model is a 3D Chemical  
 147 Transport Model that simulates trace gas and aerosol concentrations in the lower troposphere (Manders, Bultjes,  
 148 Curier, Denier Van Der Gon, Hendriks, Jonkers, Kranenburg, Kuenen, Segers, Timmermans, Visschedijk, Kruit, Addo,  
 149 Van Pul, Sauter, Van Der Swaluw, Swart, Douros, Eskes, Van Meijgaard, Van Ulft, Van Velthoven, Banzhaf, Mues,  
 150 Stern, Fu, Lu, Heemink, Van Velzen and Schaap, 2017). The simulated concentrations include ozone, particulate  
 151 matter, nitrogen dioxide, heavy metals, and organic components (Sauter, der Swaluw, Manders-groot, Kruit, Segers  
 152 and Eskes, 2012). The physical processes in the model include emission, advection, diffusion, chemical reactions, and

153 dry and wet deposition. The input to the LOTOS-EUROS model mainly consists of meteorological data, emission  
 154 inventories, and surface data such as land-use and vegetation type. LOTOS-EUROS has demonstrated its capacity  
 155 through a wide use in different projects around the world (Manders, Schaap and Hoogerbrugge, 2009; Curier, Timmer-  
 156 mans, Calabretta-Jongen, Eskes, Segers, Swart and Schaap, 2012; Mues, Kuenen, Hendriks, Manders, Segers, Scholz,  
 157 Hueglin, Bultjes and Schaap, 2014; Fu, Heemink, Lu, Segers, Weber and Lin, 2016; Jin, Lin, Heemink and Segers,  
 158 2018; Lopez-Restrepo et al., 2020). For a full description of the physical processes and input data could be found in  
 159 Manders et al. (2017).

160 Two different time periods were selected to analyze the model performance using the new emission inventory. The  
 161 first period covered 8-25 January 2019 which represents cases with moderate concentration that are close to the annual  
 162 mean. The second period covered 25-February through 15-March which represents cases with high concentrations,  
 163 related to overpass of the ITCZ. The spatial domains and the summarize of the experimental setup are presented in the  
 164 Table 1 For each period, two simulations were performed using different anthropogenic emission inventories for the  
 165 inntermost domain (D4): either EDGAR V4.3, or the disaggregated AMVA inventory.

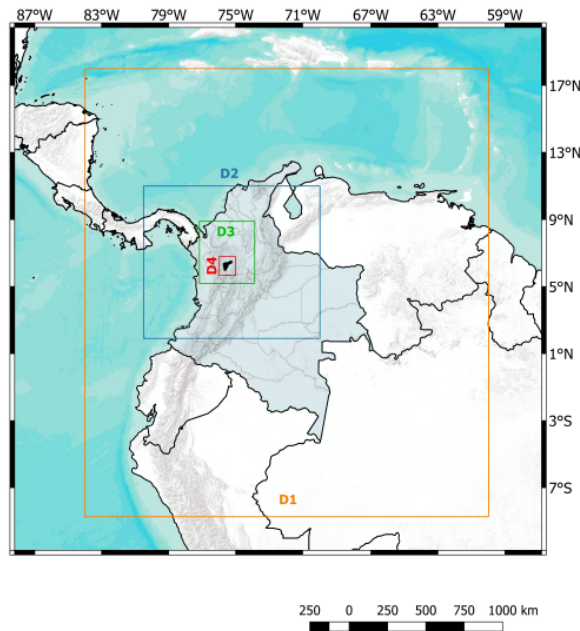


Figure 6: LOTOS-EUROS model nested domains for Metropolitan Area of Aburrá Valley assessment.

166 **2.5. Ground based sensor network and Performance metrics for validations**

167 The Sistema de Alerta Temprana del Valle de Aburrá (SIATA, [www.siata.gov.co](http://www.siata.gov.co)) is a sensor network that pro-  
 168 vides automatic and high-quality measurements of air pollutant concentrations in the metropolitan area of the Aburrá  
 169 Valley. The observed species include O<sub>3</sub>, SO<sub>2</sub>, PM<sub>10</sub>, PM<sub>2.5</sub> and PM<sub>1</sub>. The network consist of 9 stations measuring  
 170 PM<sub>10</sub>, and 21 stations measuring PM<sub>2.5</sub>. The distribution of the stations across the Aburrá Valley is shown in Figure 5.  
 171 The PM<sub>2.5</sub> and PM<sub>10</sub> equipment consists of Met One Instruments BAM-1020 and BAM-1022 monitors using a beta  
 172 ray attenuation method to measure airborne PM concentration levels (Hoyos et al., 2019). In this study, the PM<sub>10</sub> and  
 173 PM<sub>2.5</sub> stations selected for validation should have at least 70% data coverage for the periods of interest.

174 Three different metrics are used to compare observations from ground stations with simulations of the LOTOS-  
 175 EUROS model.

- 176 • The *mean fractional bias* (MFB) normalizes the bias between observation and simulations using division by the

## Spatial Disaggregation of Particulate Matter Emissions

Domain	Longitude	Latitude	Cell size	Approx. resolution
<b>D1</b>	84°W-60°W	8.5°S-18°N	0.27° × 0.27°	28 km
<b>D2</b>	80.5°W-70°W	2°N-11°N	0.09° × 0.09°	9 km
<b>D3</b>	77.2°W-73.9°W	5.2°N-8.9°N	0.03° × 0.03°	3 km
<b>D4</b>	76°W-75°W	5.7°N-6.8°N	0.01° × 0.01°	1 km
<b>Meteorology</b>	ECMWF D1 = Temp. Res.: 3h; Spat. Res.: 0.14° × 0.14° D2-4 = Temp. Res.: 3h; Spat. Res.: 0.07° × 0.07°			
<b>Initial and boundary conditions</b>	LOTOS-EUROS. (D3). Temp.res:1h Spat.Res: 0.03° × 0.03°			
<b>Biogenic emissions</b>	MEGAN. Spat. Res.: 10 km × 10 km			
<b>Fire emissions</b>	GFAS. Spat. Res.: 10 km × 10 km			
<b>Landuse</b>	GLC2000. Spat. Res.: 1km × 1km			
<b>Orography</b>	GMTED2010. Spat. Res.: 0.002°×0.002°			

**Table 1**

Nested domain specifications and model inputs for LOTOS-EUROS simulations. Simulation results from D4 were used to evaluate the impact of the disaggregated emissions inventory on model performance.

177 average of the model and observation before taking the sample mean (Boylan and Russell, 2006):

$$\text{MFB} = \frac{2}{M} \sum_{i=1}^M \frac{(y^{LE})_i - y_i^o}{(y^{LE})_i + y_i^o} \quad (2)$$

178 where  $M$  is the number of observations,  $y_i^{LE}$  is the model simulation output, and  $y_i^o$  is the observation.

- The *root mean square error* (RMSE) represents the sample standard deviation of the differences between predicted values and observed values (Zhang, Roussel, Boniface, Cuong Ha, Frappart, Darrozes, Baup and Calvet, 2017):

$$\text{RMSE} = \sqrt{\frac{1}{M} \sum_{i=1}^M ((y^{LE})_i - y_i^o)^2} \quad (3)$$

179 The RMSE penalizes a high variance as it gives errors with larger absolute values more weight than errors with  
180 smaller absolute values (Chai and Draxler, 2014).

- The last metric used is the *correlation factor* (CF), which shows how the values from one data set (simulations) relate to the value of a second data set (observations). The correlation coefficient is calculated following:

$$\text{CF} = \frac{\sum_{i=1}^M \left( (y^{LE})_i - \overline{(y^{LE})} \right) \left( y_i^o - \overline{y^o} \right)}{\sqrt{\sum_{i=1}^M \left( (y^{LE})_i - \overline{(y^{LE})} \right)^2} \sqrt{\sum_{i=1}^M \left( y_i^o - \overline{y^o} \right)^2}} \quad (4)$$

181 where the overline denotes a sample mean over the  $M$  elements.

### 182 3. Results

183 Using the disaggregation methodology described in Section 2.3 with the data presented in Section 2.1, a local  
184 emission inventory suitable for model simulation was obtained. To carry out a complete evaluation of the new AMVA  
185 emission inventory, different types of comparisons were made. First, a comparison between the total emissions and  
186 the spatial distribution in the AMVA and EDGAR V4.3 inventories is made in sections 3.1 and 3.2. This comparison  
187 evaluates the spatial representativeness of the new emissions inventory and compares it to the global inventory. Second,



188 an evaluation of the LOTOS-EUROS model using both emission inventories as input is made in sections 3.3 and  
 189 3.4. A comparison is made between the simulated particulate matter concentrations and the observations from the  
 190 SIATA network. Evaluating the modeled concentrations, it was possible to assess the performance of the new emission  
 191 inventory and to identify the most important improvements when this data is used instead of the global inventory.

192 **3.1. Comparison of global and local traffic emissions**

193 Traffic emissions represent the largest urban source of PM<sub>2.5</sub> Zavala, Barrera, Morante and Molina (2013); Pre-  
 194 malatha Kanikannan and Duraiswamy (2014); Ferm and Sjöberg (2015). For the considered domain, about 80% of  
 195 the total PM<sub>2.5</sub> emissions can be attributed to traffic, as shown in Figure 2. Figure 7 shows a comparison between the  
 196 local AMVA emissions inventory and the global emission inventory EDGAR V4.3 for traffic PM<sub>2.5</sub> emissions. For  
 197 EDGAR V4.3, the map shows section "1A3b" that corresponds with road transportation (Crippa et al., 2018).

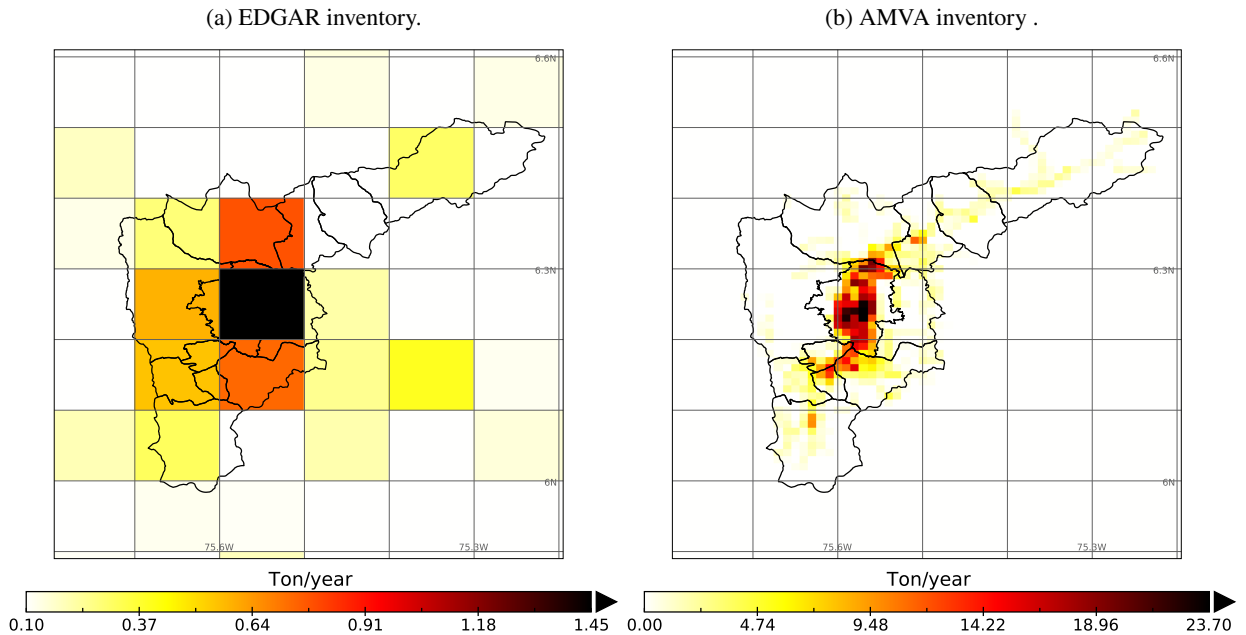


Figure 7: PM<sub>2.5</sub> on-road annual emissions in (a) EDGAR v4.3 and (b) AMVA inventory.

198 The AMVA inventory has a much higher spatial resolution (1x1 km) than EDGAR (10x10 km). Although this does  
 199 not necessarily mean an improvement in accuracy, a higher resolution does allow a more detailed spatial representation  
 200 of emissions. The spatial resolution is especially important for the Aburrá Valley since it has a complicated topography  
 201 (a narrow and deep valley) with emissions concentrated in a rather small area.

202 In the low resolution emission map of EDGAR, on-road emissions are assigned to locations in the eastern part of  
 203 the city of Medellín (located in the center of the valley, see Figure 5) and to the grid cells north and south of it, which  
 204 are mainly rural zones. This coarse representation does not allow to differentiate the main road corridors or the areas  
 205 characterized by high vehicular flow in the city. González et al. (2018) observed a similar situation for the Colombian  
 206 city of Manizales.

207 The disaggregated AMVA inventory provides a more detailed representation of the city's traffic network. In this  
 208 inventory, it was possible to differentiate the main vehicular artery that traverses the valley from south to north-east.  
 209 The largest share of emissions is concentrated in the center of the city of Medellín (largest urban hub in the metropolitan  
 210 area), and along its Southern borders with Envigado, Sabaneta, and Itagui (see Figure 5), a location characterized by  
 211 high vehicular traffic and frequent congestion. The use of a simplified road map instead of the complete map avoided  
 212 over-estimation of traffic emission in the residential areas located on the slopes of the valley, which are characterized  
 213 by high road density but low vehicle flow.

214 In terms of total emissions for the region, the EDGAR inventory estimates a total PM<sub>2.5</sub> emission from road traffic  
 215 that is approximately 18 times lower than the estimate in the by AMVA inventory. The lower total suggest that the

216 EDGAR inventory might underestimate emissions from the transportation sector in midsize cities compared to their  
 217 upstream and local emissions inventories (Gonzalez et al., 2017).

### 218 3.2. Comparison of industrial point-source emissions

219 Figure 8 shows a comparison between the PM<sub>10</sub> industrial point-source emissions from the disaggregated AMVA  
 220 inventory, and EDGAR v4.3 (combustion for manufacturing 1A2, chemical processes 2B, food and paper 2D, and iron  
 221 and steel production (Crippa et al., 2018)).

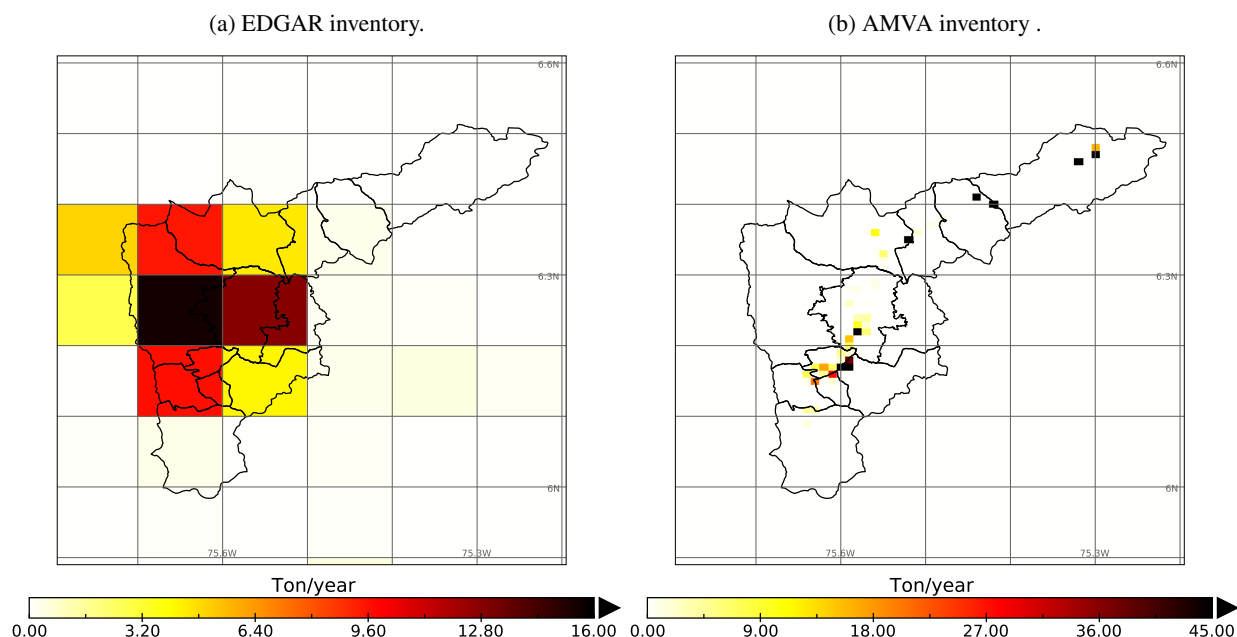


Figure 8: PM<sub>10</sub> industrial point-source emissions in (a) EDGAR v4.3 and (b) AMVA inventory.

222 Industrial sources are the major contributors to PM<sub>10</sub> emissions as shown in Figure 2. The Metropolitan Area of the  
 223 Aburrá Valley has a well-defined distribution of industrial facilities, located mainly in the center and the Southwestern  
 224 part of the city of Medellín and the municipality of Itagüí. The north of the valley hosts mainly quarries and mines for  
 225 the extraction of construction material. The high resolution of the AMVA inventory has the advantage of being able  
 226 to accurately represent the location of the industrial sources, where the EDGAR resolutions only allow a very crude  
 227 spatial assignment. In the global inventory, the main source of industrial emissions appears on the western flank of the  
 228 Valley, which is actually mainly a residential or even rural area.

229 In terms of total PM<sub>10</sub> emissions, the EDGAR estimate is very similar to the values estimated by AMVA. Although  
 230 EDGAR is known to overestimate industrial emissions of gases such as NVMOC, CO, and NO<sub>x</sub> in the Colombian city  
 231 of Manizales (Gonzalez et al., 2017; González et al., 2018), this seems not the case for the the Aburrá Valley. For  
 232 PM<sub>2.5</sub>, EDGAR estimate exceeds the AMVA with a factor 10.

### 233 3.3. Simulated concentrations

234 The difference in representation of PM emissions between the high-resolution local inventory and the coarse-  
 235 resolution global emission has been evaluated using simulations with the LOTOS-EUROS CTM. Two simulations  
 236 were carried out using different inventories for PM<sub>2.5</sub> and PM<sub>10</sub>, while the remaining species (e.g., NO<sub>x</sub>, CO, SO<sub>x</sub>),  
 237 were taken from EDGAR v4.3 in both cases. In the first simulation the disaggregated high-resolution local emission  
 238 inventory was used as described in Subsection 2.3 (hereafter referred to as the LE-AMVA simulation); in the second  
 239 simulation, the global emission inventory EDGAR v4.3 was used (LE-EDGAR simulation).

240 Time series of simulated concentrations are shown in figures 9 and 10 for four stations each. The diurnal cycles  
 241 are shown in figures 11 and 12 for the same stations. The selected stations are located in the north (stations 3, and 11  
 242 ), center (stations 25, 28, 6, and 74), and south of the valley (stations 90, and 48) as marked in Figure 5. The stations  
 243 are representative for residential areas (stations 3, 11, 74, and 90), highways and areas of high vehicular flow (stations

244 6, 25, and 28), or an industrial area (48). Figures 14 and 13 show a comparison between the MFB, RMSE, and CF  
 245 measures for all stations with data available.

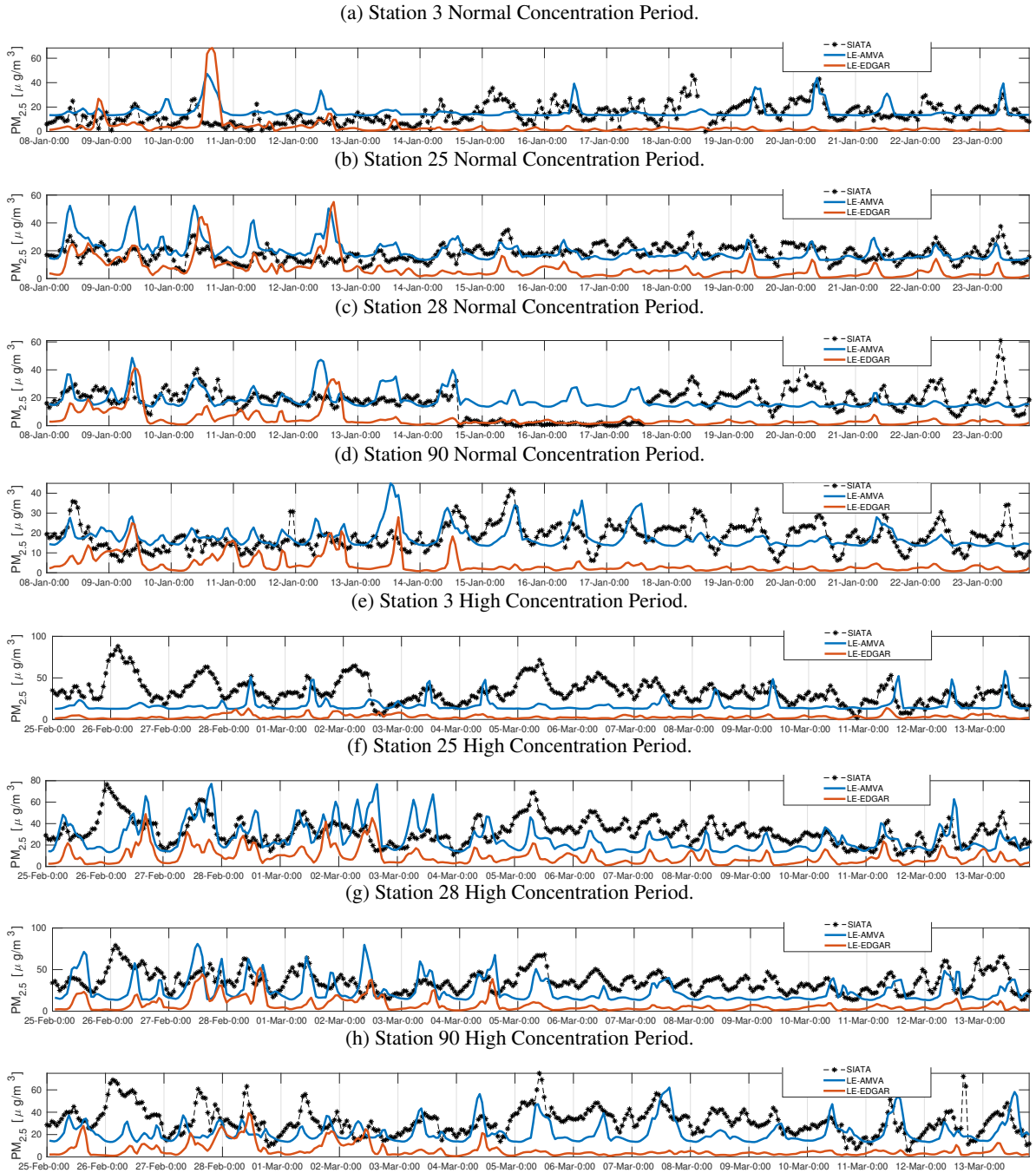
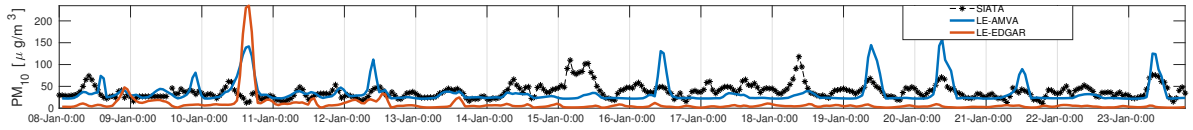


**Figure 9:** Comparison of LE-AMVA and LE-EDGAR  $PM_{2.5}$  concentration against SIATA observations for both concentrations period. The time axis corresponds with the local time zone UTC-5.

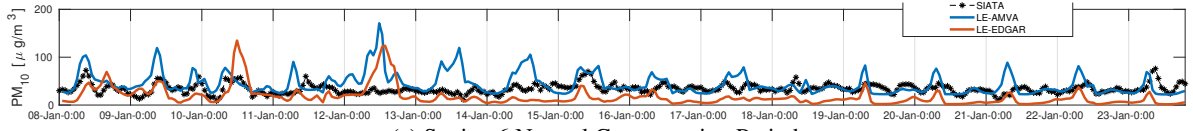
246 In general, the model performance improved significantly with the use of the local inventory compared to the results  
 247 obtained using the global inventory. The LE-EDGAR simulation consistently underestimated the concentrations of  
 248  $PM_{2.5}$  in all the stations analyzed (Figure 9, and Figure 13 (d) and (j)). The MFB values reported for LE-EDGAR  
 249 in the *Normal Concentration Period* (Figure 13 (d)) remain around -1.0 and -1.2, and for the *High Concentration*

## Spatial Disaggregation of Particulate Matter Emissions

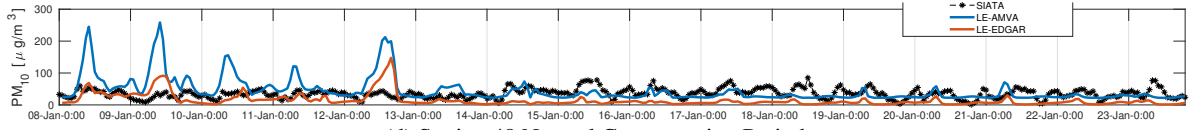
(a) Station 11 Normal Concentration Period.



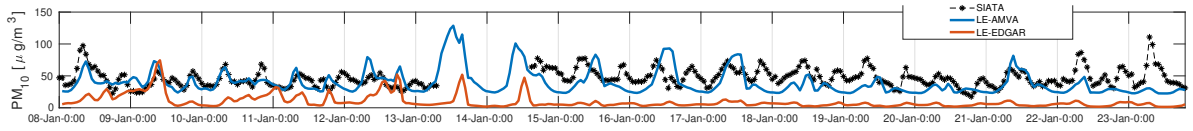
(b) Station 74 Normal Concentration Period.



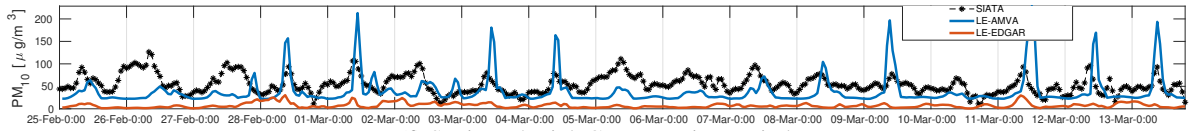
(c) Station 6 Normal Concentration Period.



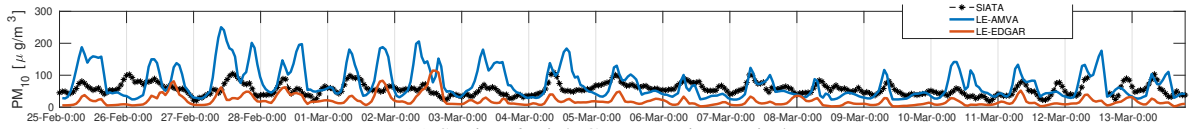
(d) Station 48 Normal Concentration Period.



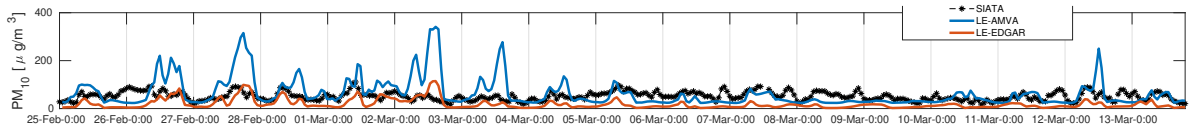
(e) Station 11 High Concentration Period.



(f) Station 74 High Concentration Period.



(g) Station 6 High Concentration Period.



(h) Station 48 High Concentration Period.

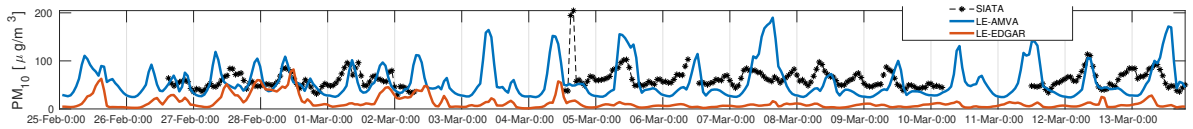


**Figure 10:** Comparison of LE-AMVA and LE-EDGAR  $PM_{10}$  concentration against SIATA observations for both concentrations period. The time axis corresponds with the local time zone UTC-5.

250 *Period* between -1.3 and -1.6 (Figure 13 (j)). However, LE-AMVA simulations provided concentrations much closer  
 251 to the observations (Figure 9, and Figure 13 (a) and (g)). An underestimation is often still present, but much reduced  
 252 compared to LE-EDGAR, and in some cases concentrations are even higher than observed. The LE-AMVA simulation  
 253 provides MFB values between -0.1 and 0.1 in the normal concentration period (Figure 13 (a)) and between -0.1 and -0.3  
 254 in the high concentration period (Figure 13 (g)). Underestimations are therefore larger during the high concentration  
 255 period. This could be explained from poor meteorological representations of the conditions that caused the increase

## Spatial Disaggregation of Particulate Matter Emissions

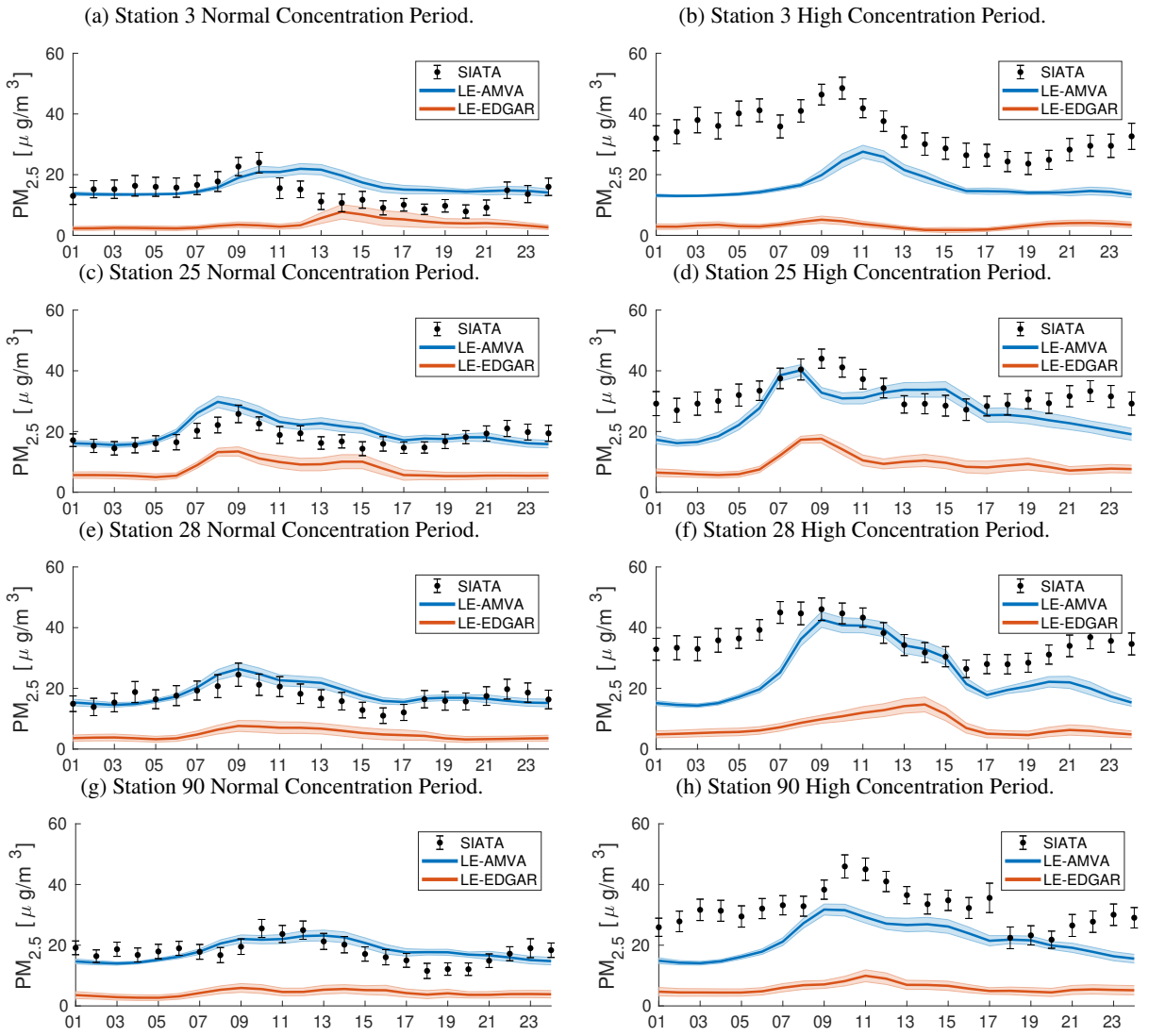


**Figure 11:** Comparison of LE-AMVA and LE-EDGAR  $PM_{2.5}$  daily cycle against SIATA observations for both concentrations periods. The time axis corresponds with the local time zone UTC-5.

in pollutant levels inside the valley, such as a low boundary layer height, high cloudiness, and increased atmospheric stability ((Herrera-Mejía and Hoyos, 2019; Roldán-Henao, Hoyos, Herrera-Mejía and Isaza, 2020)).

Representation of the temporal variability in  $PM_{2.5}$  concentrations improved when the local inventory was used. RMSE values were lower for LE-AMVA than for LE-EDGAR (Figure 13 (b), (e), (h), and (k)), and like the MFB, they were higher in the high concentration period for both cases. Both configurations represented the diurnal variability rather accurate, with LE-AMVA simulations approaching the observations more closely than LE-EDGAR. During the *normal concentration period* the LE-AMVA simulations captured the highest peak in concentrations at around 09:00 (Figure 11 (a), (c), (e), and (g)), with a slight overestimation of the concentration between 11:00 and 17:00. During the *high concentration period* (Figure 11 (b), (d), (f), and (h)), pollutants remain trapped in the valley due to the high atmospheric stability, which generates higher concentrations in the afternoon Henao, Mejía, Rendón and Salazar (2020), the reason why LE-AMVA reproduces better this temporal variability (although not in terms of magnitude). While both LE-AMVA and LE-EDGAR are able to capture the daily cycle, the correlation factors CF shown in Figure 13 are lower than 0.5 what is usually declared as needed for good correlation (Chang and Hanna, 2004; Shaocai, Brian, Robin, Shao-Hang and E., 2006; Boylan and Russell, 2006). The low CF values arise because the representation of the

## Spatial Disaggregation of Particulate Matter Emissions

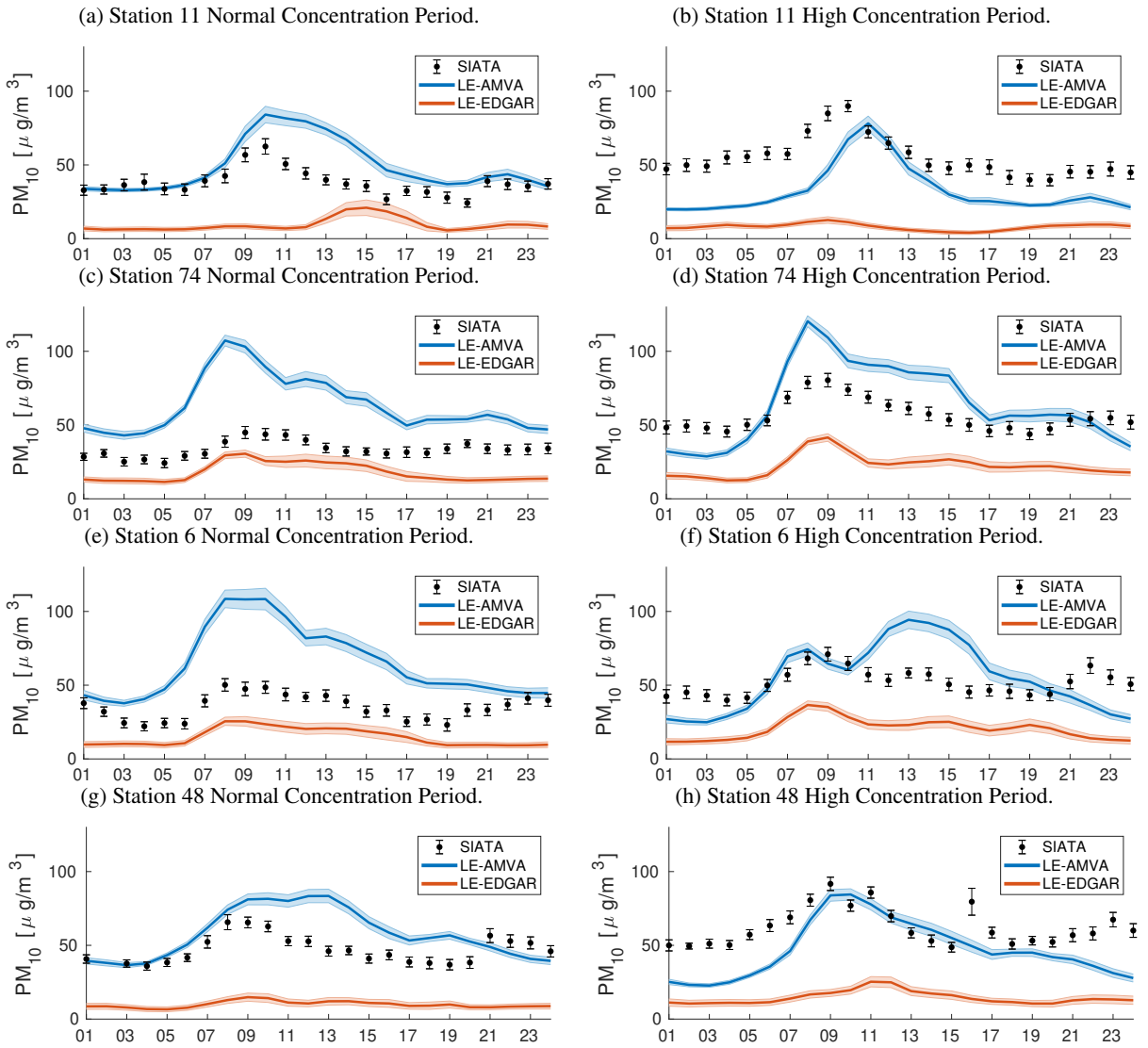


**Figure 12:** Comparison of LE-AMVA and LE-EDGAR  $PM_{10}$  daily cycle against SIATA observations for both concentrations period. The time axis corresponds with the local time zone UTC-5.

270 day-to-day or long term variability model is less accurate. In spite of this, the CF values for LE-AMVA are higher than  
 271 for LE-EDGAR. For both inventories, there is a higher correlation in the high concentration period, possibly generated  
 272 by the better representation of the daily cycle mentioned above.

273 Similar to  $PM_{2.5}$ , LE-AMVA represents  $PM_{10}$  better than LE-EDGAR. The temporal behavior of  $PM_{10}$  is similar to  
 274 that of  $PM_{2.5}$ . Both LE-AMVA and LE-EDGAR captured essential patterns of the  $PM_{10}$  day cycle in the two simulated  
 275 periods, such as the peak of the highest concentration around 09:00 and the low levels at night (Figure 12). The CF  
 276 values improved with the use of the AMVA inventory, presenting higher values than for  $PM_{2.5}$  (compare figures 13  
 277 and 14). The day-to-day variability was better captured for  $PM_{10}$  than for  $PM_{2.5}$ . In terms of magnitude, LE-EDGAR  
 278 underestimated  $PM_{10}$  levels (Figures 10, 12 and 14 (d), (j)). Similar results were reported in (Kumar et al., 2016;  
 279 González et al., 2018)) for Bogotá and Manizales. On the other hand, in some cases the LE-AMVA simulated  $PM_{10}$   
 280 concentrations are much higher than the observations (Figures 10, 12 and 14 (a), (g)), which suggest an overestimation  
 281 in the  $PM_{10}$  emissions reported by AMVA. This is likely to originate from the industrial sector, which represents about  
 282 80 % of total  $PM_{10}$  emissions (see Figure 2). As expected, the overestimation of  $PM_{10}$  levels is smaller in the period  
 283 of high concentrations due to the increase in the observed value.

## Spatial Disaggregation of Particulate Matter Emissions

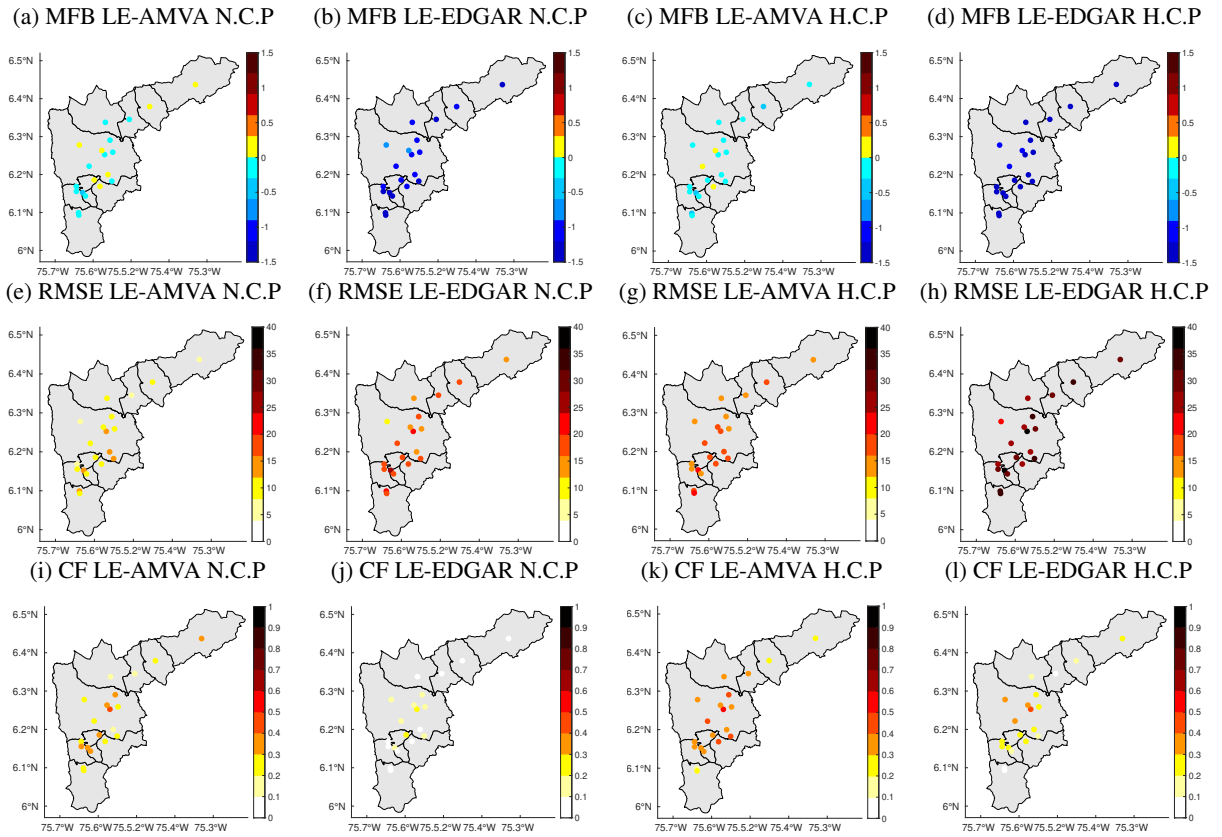


**Figure 13:** Statistical evaluation of the LOTOS-EUROS model using EDGAR v4.3 and AMVA inventory. The performance metrics were calculated over the 19 stations of  $PM_{2.5}$  with enough data available for both periods shown in Figure 5. N.C.P and H.C.P refer to Normal and High Concentration Period respectively.

### 284 3.4. Simulated PM spatial distribution

285 Figure 15 shows maps of  $PM_{2.5}$  concentrations averaged over the simulated periods. Similar figures for  $PM_{10}$  are  
 286 omitted since these are highly similar to the  $PM_{2.5}$  results, while also the greater density of the  $PM_{2.5}$  monitoring  
 287 network (21 monitoring stations versus 9 for  $PM_{10}$ ) makes an analysis for  $PM_{2.5}$  most useful. A strongly improved  
 288 spatial resolution has been obtained using the LE-AMVA simulations due to the higher spatial accuracy in positioning  
 289 of point-source and road emissions. As mentioned above, EDGAR placed emissions hot-spots in the center and west  
 290 of Medellín in mostly rural areas. Figures 15 (b) and (d) show the highest concentrations in these areas, which does  
 291 not correspond to the values measured by the SIATA station located there (station 85 see Figure 5). Figures 15 (a)  
 292 and (c) show that LE-AMVA obtained a better spatial representation, with the highest concentrations located in the  
 293 center of the city of Medellín and around its main roads, in accordance with observations. In spite this, some significant  
 294 discrepancies still appear, especially in the southern part of the metropolitan area. Stations 31 and 69 (Figure 5) present  
 295 much higher values than those reported by LE-AMVA for the same locations in both simulated periods.

### 296 4. Conclusions

297 A spatial and temporal disaggregation of the official particulate matter emission inventory of the Metropolitan Area  
 298 of the Aburrá Valley has been created. The spatial domain of this new AMVA inventory is centered over the Aburrá  
 299 Valley at a high resolution of  $1 \text{ km} \times 1 \text{ km}$ .

300 The emission distribution factors for traffic emissions were calculated using a top-down methodology based on the  
 301 road density, since actual traffic intensities are hardly available. For industrial point sources, actual locations are used.  
 302 The higher resolution has led to a more detailed spatial representation of emissions. Despite the simple methodology,  
 303 the AMVA inventory represents accurately the known hot-spots and high emissions regions for both on-road and point-

## Spatial Disaggregation of Particulate Matter Emissions

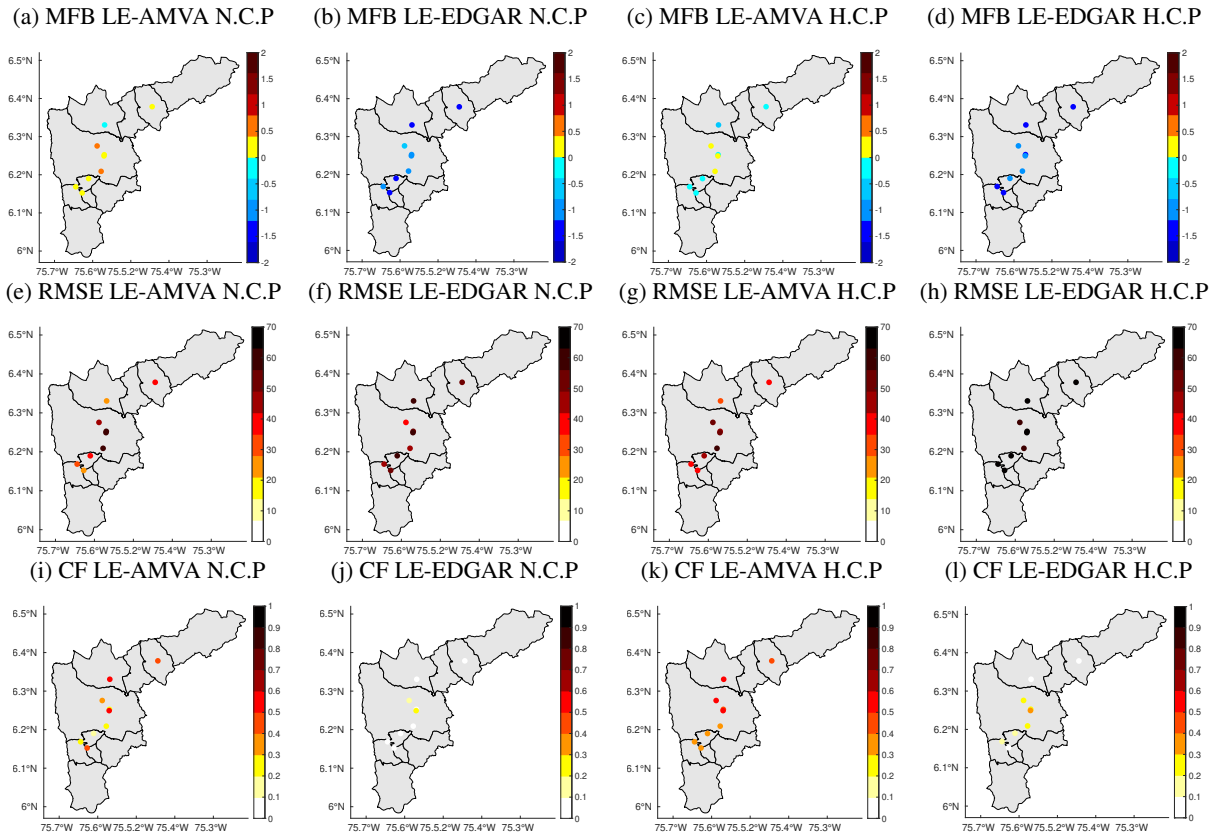


**Figure 14:** Statistical evaluation of the LOTOS-EUROS model using EDGAR V4.3 and AMVA inventory. The performance metrics were calculated over the 9 stations of  $PM_{10}$  with enough data available for both periods shown in Figure 5. N.C.P and H.C.P correspond with normal and high concentration period respectively.

304 source industrial emissions.

305 Simulations with the LOTOS-EUROS model were performed using the both the global emission inventory EDGAR  
 306 v4.3 and the new AMVA inventory, validating the results against the SIATA sensor network. The model simulations  
 307 were evaluated in two different scenarios, a period of normal or average concentrations and a period of high concen-  
 308 trations. The simulated concentrations of  $PM_{10}$  and  $PM_{2.5}$  showed strongly improved representation of observations  
 309 when the AMVA inventory was used. Particulate matter simulations were closer to observations with the AMVA  
 310 inventory, reducing Mean-Fractional-Bias (MFB) and Root Mean Square Error (RMSE) during both episodes. The  
 311 correlation between the modelled concentrations and the observations increased with the new emissions inventory for  
 312 both size ranges and scenarios.

313 The results highlight the importance of detailed emissions information in regions where the global inventories are  
 314 not accurate, as is the case for Colombia. Even simple methodologies as the one employed here could strengthen the  
 315 capacity to represent and understand the dynamical behaviour of air pollution in complex cities.

316 An interesting future work, which is outside the scope of this paper, would be to implement data assimilation  
 317 techniques to improve the model performance and correct model uncertainties in the emissions inventory and mete-  
 318 orological fields. The new high-resolution disaggregated AMVA inventory will support ongoing efforts to quantify  
 319 exposure to air pollution in Medellín and surrounding area.



## Spatial Disaggregation of Particulate Matter Emissions

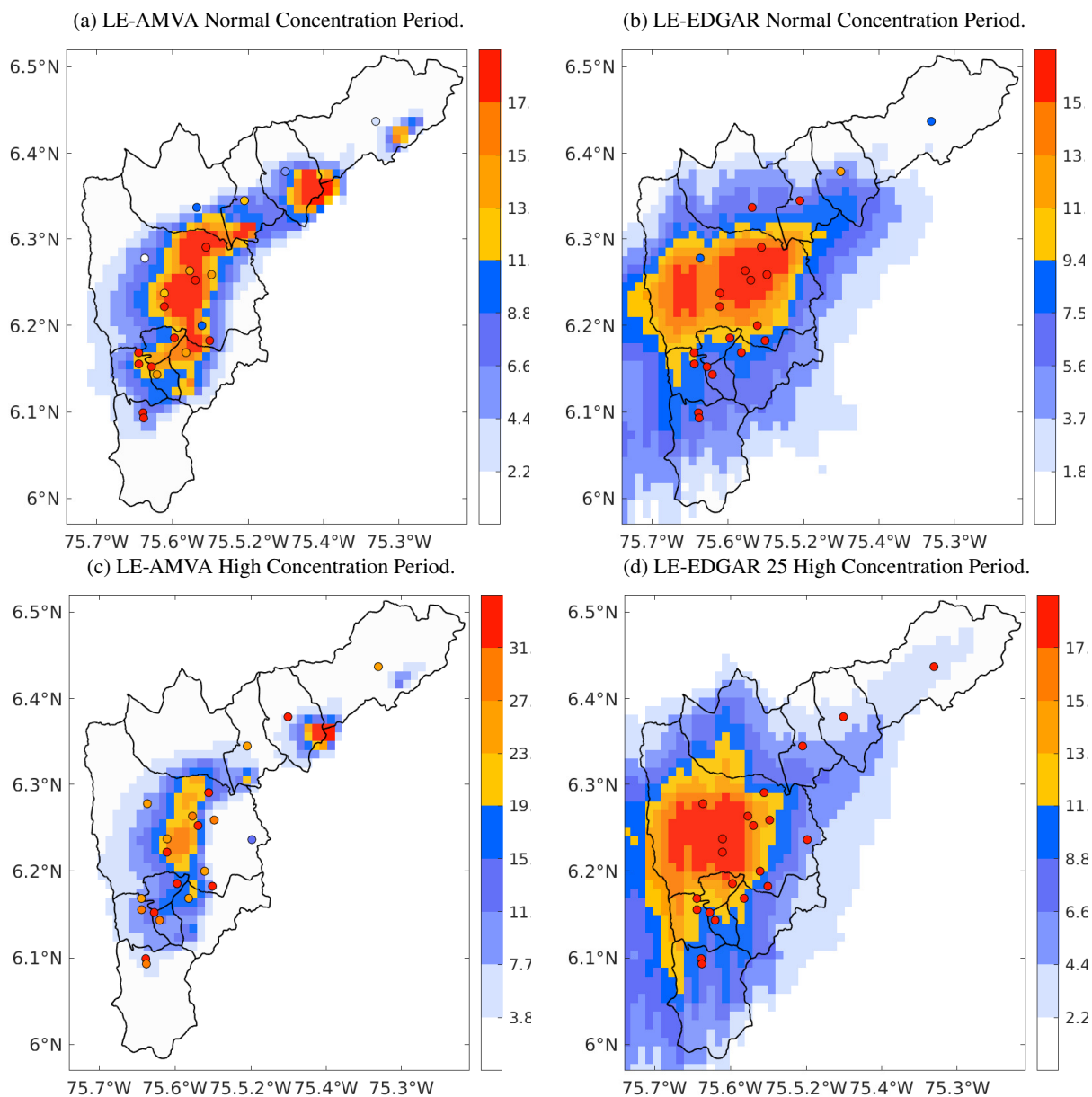


**Figure 15:** Comparison of LE-AMVA and LE-EDGAR  $PM_{2.5}$  simulations averaged over periods of simulation. The circles represent the SIATA stations. The color scales are different to distinguish the spatial dynamics of each model simulation.

### 320 CRediT authorship contribution statement

321 **Santiago Lopez-Restrepo:** Conceptualization, Methodology, Software, Writing - Original Draft. **Andres Yarce:**  
322 Methodology, Software. **Nicolás Pínel:** Conceptualization, Methodology, Writing - Review & Editing. **O. L. Quintero:**  
323 Conceptualization, Methodology, Writing - Original Draft- Review & Editing, Supervision. **Arjo Segers:**  
324 Methodology, Software, Writing - Review & Editing. **A. W. Heemink:** Writing - Review & Editing, Supervision.

### 325 References

326 Boylan, J.W., Russell, A.G., 2006. Pm and light extinction model performance metrics, goals, and criteria for three-dimensional air quality models.  
327 Atmospheric Environment 40, 4946 – 4959. doi:<https://doi.org/10.1016/j.atmosenv.2005.09.087>. special issue on Model Evaluation:  
328 tion: Evaluation of Urban and Regional Eulerian Air Quality Models.

## Spatial Disaggregation of Particulate Matter Emissions

- 329 Chai, T., Draxler, R.R., 2014. Root mean square error (rmse) or mean absolute error (mae): Arguments against avoiding rmse in the literature.  
330 Geoscientific Model Development 7, 1247–1250. doi:10.5194/gmd-7-1247-2014.
- 331 Chang, J.C., Hanna, S.R., 2004. Air quality model performance evaluation. *Meteorology and Atmospheric Physics* 87, 167–196. doi:10.1007/  
332 s00703-003-0070-7.
- 333 Crippa, M., Guizzardi, D., Muntean, M., Schaaf, E., Dentener, F., van Aardenne, J.A., Monni, S., Doering, U., Olivier, J.G.J., Pagliari, V., Janssens-  
334 Maenhout, G., 2018. Gridded emissions of air pollutants for the period 1970–2012 within edgar v4.3.2. *Earth System Science Data* 10, 1987–  
335 2013. URL: <https://www.earth-syst-sci-data.net/10/1987/2018/>, doi:10.5194/essd-10-1987-2018.
- 336 Curier, R.L., Timmermans, R., Calabretta-Jongen, S., Eskes, H., Segers, A., Swart, D., Schaap, M., 2012. Improving ozone forecasts over Europe  
337 by synergistic use of the LOTOS-EUROS chemical transport model and in-situ measurements. *Atmospheric Environment* 60, 217–226. doi:10.  
338 1016/j.atmosenv.2012.06.017.
- 339 Ferm, M., Sjöberg, K., 2015. Concentrations and emission factors for PM<sub>2.5</sub> and PM<sub>10</sub> from road traffic in Sweden. *Atmospheric Environment*  
340 119, 211–219. doi:10.1016/j.atmosenv.2015.08.037.
- 341 Fu, G., Heemink, A., Lu, S., Segers, A., Weber, K., Lin, H.X., 2016. Model-based aviation advice on distal volcanic ash clouds by assimilating  
342 aircraft in situ measurements. *Atmospheric Chemistry and Physics* 16, 9189–9200. doi:10.5194/acp-16-9189-2016.
- 343 Gómez, C.D., González, C.M., Osses, M., Aristizábal, B.H., 2018. Spatial and temporal disaggregation of the on-road vehicle emission inventory  
344 in a medium-sized Andean city. Comparison of GIS-based top-down methodologies. *Atmospheric Environment* 179, 142–155. URL: <https://doi.org/10.1016/j.atmosenv.2018.01.049>, doi:10.1016/j.atmosenv.2018.01.049.
- 345  
346 Gonzalez, C.M., Gomez, C.D., Rojas, N.Y., Acevedo, H., Aristizabal, B.H., 2017. Relative impact of on-road vehicular and point-source industrial  
347 emissions of air pollutants in a medium-sized Andean city. *Atmospheric Environment* 152, 279–289. doi:10.1016/j.atmosenv.2016.12.  
348 048.
- 349 González, C.M., Ynoue, R.Y., Vara-Vela, A., Rojas, N.Y., Aristizábal, B.H., 2018. High-resolution air quality modeling in a medium-sized city in  
350 the tropical Andes: Assessment of local and global emissions in understanding ozone and PM<sub>10</sub> dynamics. *Atmospheric Pollution Research* ,  
351 1–15doi:10.1016/j.apr.2018.03.003.
- 352 Green, J., Sánchez, S., 2012. Air Quality in Latin America: An Overview. Technical Report. Clean air Institute. Washington D.C., USA. doi:10.  
353 1017/CB09781107415324.004.
- 354 Haklay, M., Weber, P., 2008. Openstreetmap: User-generated street maps. *IEEE Pervasive Computing* 7, 12–18.
- 355 Henao, J.J., Mejía, J.F., Rendón, A.M., Salazar, J.F., 2020. Sub-kilometer dispersion simulation of a co tracer for an inter-andean urban valley.  
356 *Atmospheric Pollution Research* 11, 928 – 945. doi:<https://doi.org/10.1016/j.apr.2020.02.005>.
- 357 Herrera-Mejía, L., Hoyos, C.D., 2019. Characterization of the atmospheric boundary layer in a narrow tropical valley using remote-  
358 sensing and radiosonde observations and the wrf model: the aburrá valley case-study. *Quarterly Journal of the Royal Meteorological*  
359 *Society* 145, 2641–2665. URL: <https://rmets.onlinelibrary.wiley.com/doi/abs/10.1002/qj.3583>, doi:10.1002/qj.3583,  
360 arXiv:<https://rmets.onlinelibrary.wiley.com/doi/pdf/10.1002/qj.3583>.
- 361 Hoyos, C.D., Herrera-Mejía, L., Roldán-Henao, N., Isaza, A., 2019. Effects of fireworks on particulate matter concentration in a narrow val-  
362 ley: the case of the medellín metropolitan area. *Environmental Monitoring and Assessment* 192, 6. URL: [https://doi.org/10.1007/](https://doi.org/10.1007/s10661-019-7838-9)  
363 [s10661-019-7838-9](https://doi.org/10.1007/s10661-019-7838-9), doi:10.1007/s10661-019-7838-9.
- 364 Jiménez, J.F., 2016. Altura de la Capa de Mezcla en un área urbana montañosa y tropical. Caso de estudio: Valle de Aburrá (Colombia). Doctoral  
365 thesis. Universidad de Antioquia. Medellín.
- 366 Jin, J., Lin, H.X., Heemink, A., Segers, A., 2018. Spatially varying parameter estimation for dust emissions using reduced-tangent-linearization  
367 4DVar. *Atmospheric Environment* doi:10.1016/j.atmosenv.2018.05.060.
- 368 Kumar, A., Jiménez, R., Belalcázar, L.C., Rojas, N.Y., 2016. Application of WRF-Chem Model to Simulate PM<sub>10</sub> Concentration over Bogota.  
369 *Aerosol and Air Quality Research* 16, 1206–1221. doi:10.4209/aaqr.2015.05.0318.
- 370 Lateb, M., Meroney, R., Yataghene, M., Fellouah, H., Saleh, F., Boufadel, M., 2016. On the use of numerical modelling for near-field pollutant  
371 dispersion in urban environments: A review. *Environmental Pollution* 208, 271–283. doi:10.1016/j.envpol.2015.07.039.
- 372 Lopez-Restrepo, S., Yarce, A., Pinel, N., Quintero, O., Segers, A., Heemink, A., 2020. Forecasting PM<sub>10</sub> and PM<sub>2.5</sub> in the Aburrá Valley (Medellín,  
373 Colombia) via EnKF based Data Assimilation. *Atmospheric Environment* , . doi:10.1016/j.atmosenv.2020.117507.
- 374 Manders, A.M., Schaap, M., Hoogerbrugge, R., 2009. Testing the capability of the chemistry transport model LOTOS-EUROS to forecast PM<sub>10</sub>  
375 levels in the Netherlands. *Atmospheric Environment* 43, 4050–4059. doi:10.1016/j.atmosenv.2009.05.006.
- 376 Manders, A.M.M., Bultjes, P.J.H., Curier, L., Denier Van Der Gon, H.A.C., Hendriks, C., Jonkers, S., Kranenburg, R., Kuenen, J.J.P., Segers, A.J.,  
377 Timmermans, R.M.A., Visschedijk, A.J.H., Kruit, R.J.W., Addo, W., Van Pul, J., Sauter, F.J., Van Der Swaluw, E., Swart, D.P.J., Douros, J.,  
378 Eskes, H., Van Meijgaard, E., Van Ulft, B., Van Velthoven, P., Banzhaf, S., Mues, A.C., Stern, R., Fu, G., Lu, S., Heemink, A., Van Velzen, N.,  
379 Schaap, M., 2017. Curriculum vitae of the LOTOS-EUROS (v2.0) chemistry transport model. *Geosci. Model Dev* 10, 4145–4173. doi:10.  
380 5194/gmd-10-4145-2017.
- 381 Mues, a., Kuenen, J., Hendriks, C., Manders, a., Segers, a., Scholz, Y., Hueglin, C., Bultjes, P., Schaap, M., 2014. Sensitivity of air pollution  
382 simulations with LOTOS-EUROS to the temporal distribution of anthropogenic emissions. *Atmospheric Chemistry and Physics* 14, 939–955.  
383 doi:10.5194/acp-14-939-2014.
- 384 Nedbor-Gross, R., Henderson, B.H., Pérez-Peña, M.P., Pachón, J.E., 2018. Air quality modeling in Bogotá Colombia using local emissions and  
385 natural mitigation factor adjustment for re-suspended particulate matter. *Atmospheric Pollution Research* 9, 95–104. doi:10.1016/j.apr.  
386 2017.07.004.
- 387 Ossés de Eicker, M., Zah, R., Triviño, R., Hurni, H., 2008. Spatial accuracy of a simplified disaggregation method for traffic emissions applied in  
388 seven mid-sized Chilean cities. *Atmospheric Environment* 42, 1491–1502. doi:10.1016/j.atmosenv.2007.10.079.
- 389 Pachón, J.E., Galvis, B., Lombana, O., Carmona, L.G., Fajardo, S., Rincón, A., Meneses, S., Chaparro, R., Nedbor-Gross, R., Henderson, B., 2018.  
390 Development and evaluation of a comprehensive atmospheric emission inventory for air quality modeling in the megacity of Bogotá. *Atmosphere*  
391 9, 1–17. doi:10.3390/atmos9020049.

## Spatial Disaggregation of Particulate Matter Emissions

- 392 Premalatha Kanikannan, R., Duraiswamy, K., 2014. Face recognition system based on spectral graph wavelet theory. *Research Journal of Applied*  
393 *Sciences, Engineering and Technology* 8, 1456–1460. doi:10.19026/rjaset.8.1121.
- 394 Roldán-Henao, N., Hoyos, C.D., Herrera-Mejía, L., Isaza, A., 2020. An investigation of the precipitation net effect on the particulate matter  
395 concentration in a narrow valley: Role of lower-troposphere stability. *Journal of Applied Meteorology and Climatology* 59, 401–426. doi:10.  
396 1175/JAMC-D-18-0313.1.
- 397 Saide, P., Zah, R., Osses, M., Ossés de Eicker, M., 2009. Spatial disaggregation of traffic emission inventories in large cities using simplified  
398 top-down methods. *Atmospheric Environment* 43, 4914–4923. URL: <http://dx.doi.org/10.1016/j.atmosenv.2009.07.013>, doi:10.  
399 1016/j.atmosenv.2009.07.013.
- 400 Sauter, F., der Swaluw, E.V., Manders-groot, A., Kruit, R.W., Segers, A., Eskes, H., 2012. TNO report TNO-060-UT-2012-01451. Technical  
401 Report. TNO. Utrecht, Netherlands.
- 402 Shaocai, Y., Brian, E., Robin, D., Shao-Hang, C., E., S.S., 2006. New unbiased symmetric metrics for evaluation of air quality models. *Atmospheric*  
403 *Science Letters* 7, 26–34. doi:10.1002/asl.125.
- 404 Shu, Y., Lam Nina, N.S.N., 2011. Spatial disaggregation of carbon dioxide emissions from road traffic based on multiple linear regression model.  
405 *Atmospheric Environment* 45, 634–640. URL: <http://dx.doi.org/10.1016/j.atmosenv.2010.10.037>, doi:10.1016/j.atmosenv.  
406 2010.10.037.
- 407 Thunis, P., Miranda, A., Baldasano, J.M., Blond, N., Douros, J., Graff, A., Janssen, S., Juda-Rezler, K., Karvosenoja, N., Maffei, G., Martilli,  
408 A., Rasoloharimahefa, M., Real, E., Viaene, P., Volta, M., White, L., 2016. Overview of current regional and local scale air quality modelling  
409 practices: Assessment and planning tools in the EU. *Environmental Science & Policy* 65, 13–21. doi:10.1016/j.envsci.2016.03.013.
- 410 Tuia, D., Ossés de Eicker, M., Zah, R., Osses, M., Zarate, E., Clappier, A., 2007. Evaluation of a simplified top-down model for the spatial  
411 assessment of hot traffic emissions in mid-sized cities. *Atmospheric Environment* 41, 3658–3671. doi:10.1016/j.atmosenv.2006.12.045.
- 412 UPB, AMVA, 2017. Inventario de Emisiones Atmosféricas del Valle de Aburrá - actualización 2015. Technical Report. Universidad Pontificia  
413 Bolivariana - Grupo de Investigaciones Ambientales, Area Metropolitana del Valle de Aburra. Medellín. URL: <https://www.metropol.gov.co/ambiental/calidad-del-aire/Documents/Inventario-de-emisiones>.
- 414 US EPA (United State Environmental Protection Agency), 1995. AP-42: Compilation of Air Emissions Factors. Technical Report. US  
415 EPA (United State Environmental Protection Agency). URL: [https://www.epa.gov/air-emissions-factors-and-quantification/  
416 ap-42-compilation-air-emissions-factors](https://www.epa.gov/air-emissions-factors-and-quantification/ap-42-compilation-air-emissions-factors).
- 417 Zavala, M., Barrera, H., Morante, J., Molina, L.T., 2013. Analysis of model-based PM2.5 emission factors for on-road mobile sources in Mexico.  
418 *Atmosfera* 26, 109–124. doi:10.1016/S0187-6236(13)71065-8.
- 419 Zhang, S., Roussel, N., Boniface, K., Cuong Ha, M., Frappart, F., Darrozes, J., Baup, F., Calvet, J.C., 2017. Use of reflected GNSS SNR data  
420 to retrieve either soil moisture or vegetation height from a wheat crop. *Hydrology and Earth System Sciences* 21, 4767–4784. doi:10.5194/  
421 hess-21-4767-2017.
- 422